Defect-induced ferromagnetism in Mn-doped Cu_2O

2008 J. Phys.: Condens. Matter 20 215216

(http://iopscience.iop.org/0953-8984/20/21/215216)

J. Phys.: Condens. Matter **20** (2008) 215216 (5pp) doi:10.1088/0953-8984/20/21/215216

Defect-induced ferromagnetism in Mn-doped Cu_2O

G S Chang[1], E Z Kurmaev[2], D W Boukhvalov[2,3], A Moewes[1], L D Finkelstein[2], M Wei[4] and J L MacManus-Driscoll[4]

[1] Department of Physics and Engineering Physics, University of Saskatchewan, 116 Science Place, Saskatoon, SK S7N 5E2, Canada
[2] Institute of Metal Physics, Russian Academy of Sciences-Ural Division, Yekaterinburg, 620219, Russia
[3] Institute for Molecules and Materials, Radboud University, NL-6525 ED Nijmegen, The Netherlands
[4] Department of Materials Science and Metallurgy, University of Cambridge, Pembroke Street, Cambridge CB2 3QZ, UK

E-mail: gapsoo.chang@usask.ca

Received 3 December 2007, in final form 22 February 2008
Published 22 April 2008
Online at stacks.iop.org/JPhysCM/20/215216

Abstract
In an effort to understand the ferromagnetic behaviour of Cu_2O-based diluted magnetic semiconductors, the electronic structures of Mn-doped Cu_2O sintered samples have been investigated using both experimental and theoretical approaches. Mn $L_{2,3}$ x-ray emission measurements and first-principle calculations reveal that Mn-doped Cu_2O sintered at 650 and 800 °C contains Mn interstitials as well as substitutional Mn atoms, but the defect configuration depends on the sintering temperature. A reduction of T_C with sintering temperature can be explained by the appearance of an antiferromagnetic superexchange interaction between substitutional Mn atoms via oxygen.

The theoretical prediction of high-temperature ferromagnetism in magnetically doped p-type semiconductors has stimulated experimental efforts to develop a reliable methodology to synthesize diluted magnetic semiconductors (DMSs) for their practical applications to spintronics technology [1]. Among the candidates for DMS materials, cuprous oxide (Cu_2O) has shown considerable promise as a host semiconductor because it is one of only a few binary p-type semiconductors with a direct wide bandgap of 2.0 eV [2]. The high Curie temperature (T_C) of Cu_2O-based DMS systems was initially demonstrated in Al and Co codoped Cu_2O films epitaxially grown by pulsed laser deposition [3] and later in Mn-doped Cu_2O polycrystalline bulks and epitaxial thin films prepared by electro-deposition and magnetron sputtering [4, 5]. On the other hand, a low T_C of 48 K was also reported in $Cu_{1.9}Mn_{0.1}O$ films grown by pulsed laser deposition [6]. Although the latter case was revealed to be associated with the formation of secondary Mn_3O_4 phase, the inconsistent experimental results have made the origin of high T_C ferromagnetism in Cu_2O-based DMSs unclear. In particular, ferromagnetic behaviour of the Mn-doped Cu_2O system above room temperature (RT) is unique because the exchange interaction of any pairs between substitutional Mn dopants is antiferromagnetic and there are no known ferromagnetic phases with T_C above 50 K for any combinations of Mn, Cu, and O [7]. Hence, there is a growing interest in the effect of magnetic defects (antisites and/or interstitials) on ferromagnetism in Cu_2O-based DMSs. In the present paper, the electronic structure of Mn-doped Cu_2O bulk samples showing RT ferromagnetism is investigated using soft x-ray emission spectroscopy (XES) and a theoretical approach based on a linear muffin-tin orbital method with the atomic sphere approximation (LMTO-ASA).

The Mn-doped Cu_2O samples were prepared by milling a mixture of Cu_2O and Mn_2O_3 powders in an ethanol medium. The mixed powder was then pressed into $Cu_{2-x}Mn_xO$ bulk pellets (5 mm in diameter) and sintered in flowing Ar with a flow rate of 20 cm^3 min^{-1} for 24 h in alumina crucibles. The sintering temperature was set at 650 and 800 °C. The intended nominal Mn composition in Cu_2O was 1.7 at.% (equivalent to $x = 0.034$), but the energy dispersive x-ray analysis of the samples indicated a less than 1 at.% of Mn doping level [2]. The magnetic properties of samples were measured using a vibrating sample magnetometer. According to magnetization versus magnetic field curves taken at various temperatures

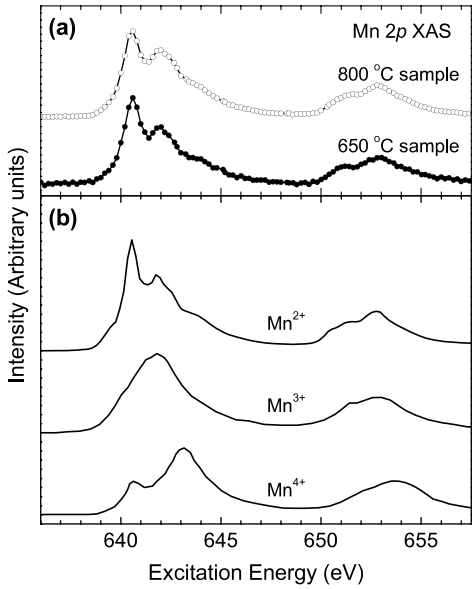

Figure 1. Mn 2p XAS spectra of (a) Mn-doped Cu_2O samples sintered at 650 (solid circles) and 800 °C (open circles), and (b) those of MnO (Mn^{2+}), norrishite (Mn^{3+}), and asbolan (Mn^{4+}).

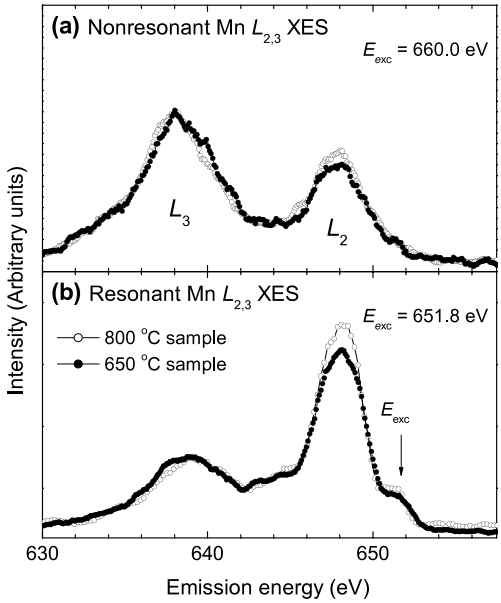

Figure 2. Mn $L_{2,3}$ nonresonant (a) and resonant (b) XES spectra of Mn-doped Cu_2O samples sintered at 650 (solid circles) and 800 °C (open circles).

(10 K $\leqslant T \leqslant$ 300 K), the sample sintered at 650 °C is found to be ferromagnetic up to RT while T_C decreases to 215 K by elevating the sintering temperature to 800 °C. The x-ray diffraction patterns of both samples clearly show typical cubic structure behaviour without any indication of a ferromagnetic secondary phase. Detailed information about the magnetic and structural properties of prepared samples is described in [2].

X-ray fluorescence measurements were carried out at Beamline 8.0.1 of the Advanced Light Source at Lawrence Berkeley National Laboratory. Both nonresonant and L_2-resonant Mn $L_{2,3}$ XES spectra were obtained at RT. In the case of resonant XES measurements, the spectra were taken at the L_2 absorption threshold with an excitation energy (E_{exc}) of 651.8 eV while nonresonant spectra were recorded at E_{exc} well above the absorption threshold (660 eV). For comparison, we also measured resonant and nonresonant XES spectra for metallic Mn and MnO reference samples. All measured spectra were normalized to the number of incident photons falling on the sample, which is monitored by a highly transparent gold mesh.

Figure 1 shows the Mn 2p XAS spectra of Mn-doped Cu_2O samples and those of reference samples having different Mn valencies (Mn^{2+} of MnO, Mn^{3+} of norrishite, and Mn^{4+} of asbolan [8]). One can see that the shape of the Mn $L_{2,3}$ absorption lines depends on the valence state of the Mn ion. The XAS spectra of Mn-doped Cu_2O samples prepared at 650 and 800 °C are very similar to that of MnO, but different from those of norrishite and asbolan. These reflect the fact that the valency of Mn impurity atoms in Cu_2O:Mn is divalent.

Nonresonant and resonant Mn $L_{2,3}$ XES spectra for Mn-doped Cu_2O samples prepared at 650 and 800 °C are presented in figure 2. The L_3 emission line (at around 638 eV) and the L_2 line (648 eV) correspond to x-ray transitions from (occupied) 3d4s valence states to $2p_{3/2}$ and $2p_{1/2}$ core holes, respectively. Higher Mn L_2 emission lines in resonant XES spectra than those in nonresonant spectra are caused by different photo-absorption coefficients (μ) depending on the excitation energy. In the case of an excitation energy well above the L_2 absorption threshold (nonresonant regime), the ratio of total photo-absorption coefficient at L_2 and L_3 thresholds (μ_2/μ_3) has a constant value while the μ_2/μ_3 becomes maximal for L_2-resonant excitation [9]. On the other hand, one can see that the relative intensity ratio of Mn L_2 to L_3 emission lines [$I(L_2)/I(L_3)$] of the 800 °C sample is higher than that of the 650 °C sample and the difference is more prominent in the resonant XES spectra. The change in the $I(L_2)/I(L_3)$ intensity ratio is related to the appearance of interstitial magnetic defects according to our previous studies on Co-doped TiO_2 and Mn-doped ZnO [9, 10]. In solid-state systems, the $I(L_2)/I(L_3)$ ratio is influenced by radiationless $L_2L_3M_{4,5}$ Coster–Kronig (CK) transitions, which correspond to radiationless electron transitions from the L_3 to the L_2 level occurring before the normal x-ray emission process. Thus, the CK transitions generally populate the L_2 core holes of the system and result in the suppression of L_2 emission. The probability of this CK process is strongly enhanced in metals containing free 3d carriers with respect to an insulating oxide because the CK transition energy is released via the emission of 3d Auger electrons [11]. This tendency is clearly illustrated by comparing the XES spectra of metallic Mn to insulating MnO as shown in figure 3. The $I(L_2)/I(L_3)$ intensity ratio is significantly reduced for metallic Mn due to the radiationless CK transitions and the L_2-resonant XES spectra show more significant reductions of the intensity ratio. Therefore, a lower $I(L_2)/I(L_3)$ ratio of the 650 °C sample than that of the 800 °C sample suggests a higher level of Mn interstitials in the 650 °C sample, contributing to direct Mn–Mn interactions.

Table 1. Calculated defect-configuration energies and magnetic properties for different defect configurations of Mn impurities in the Cu_2O cubic structure.

Defect configurations	Formation energy (eV)	$m_{Mn(S)}$ (μ_B)	$m_{Mn(I)}$ (μ_B)	$J_{Mn(S)-Mn(S)}$ (meV)	$J_{Mn(S)-Mn(I)}$ (meV)	T_C (K)
S	1.3	3.7				
$S+S$	2.7	3.63		−4		
$2S+I$ type 1	3.0	2.15	−1.02	+5	−105	408
$2S+I$ type 2	3.9	2.08	−1.29	−60	−145	218
$4S+1$	8.4	2.50	−1.16	+10	−50	505

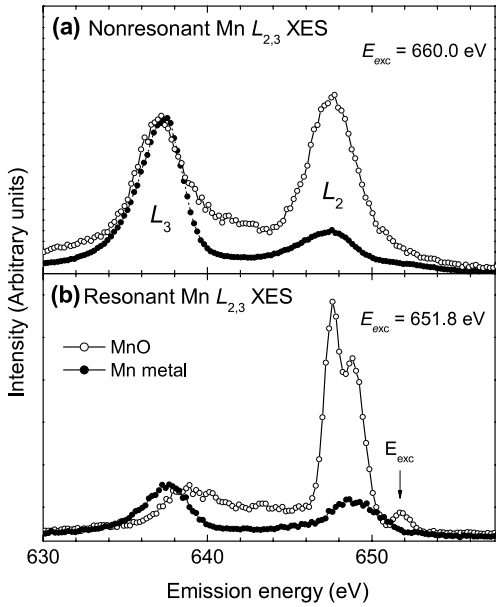

Figure 3. Mn $L_{2,3}$ nonresonant (a) and resonant (b) XES spectra of metallic Mn (solid circles) and MnO (open circles) reference samples taken at the same excitation energies as in figure 1.

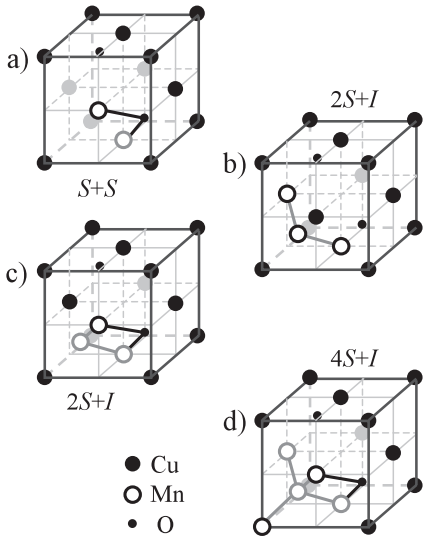

Figure 4. Schematics of various Mn-defect configurations in the Cu_2O lattice: (a) two Mn(S) atoms connected by superexchange interaction via oxygen (black lines) ($S+S$), (b) two Mn(S) and one Mn(I) atoms connected by only a direct Mn–Mn exchange interaction (gray lines) ($2S+I$ type 1), (c) same configuration in the presence of superexchange via oxygen ($2S+I$ type 2), (d) four Mn(S) and one Mn(I) atoms ($4S+I$).

As mentioned above, elevating the sintering temperature reduces the T_C of Mn-doped Cu_2O from above RT (for the 650 °C sample) to 215 K (for the 800 °C sample). If ferromagnetic behaviour of the Mn-doped Cu_2O samples stems only from the substitutional Mn dopants occupying Cu sites, the 650 °C sample must show a higher $I(L_2)/I(L_3)$ intensity ratio than the 800 °C sample. Therefore, the spectroscopic result is direct evidence that ferromagnetism in the Mn-doped Cu_2O requires the involvement of Mn interstitials. In order to understand the relation between magnetic properties of the samples and the presence of Mn interstitials, we have performed theoretical calculations for several Mn configurations in the Cu_2O lattice. We considered the following types of defect configurations (see figure 4): (a) single substitutional Mn atom, Mn(S) for a Cu site (S configuration, not shown), (b) a pair of Mn(S) atoms connected by superexchange via an oxygen atom ($S+S$ configuration in figure 4(a)), (c) two Mn(S) and one interstitial Mn atom, Mn(I) without superexchange ($2S+I$ type 1 in figure 4(b)), (d) same configuration as (c), but with consideration of superexchange ($2S+I$ type 2 in figure 4(c)), (e) four Mn(S) and one Mn(I) ($4S+I$ in figure 4(d)). For all these configurations, the electronic structure and exchange interactions are calculated using a LMTO-ASA method realized in the Stuttgart TB47 code [12]. Since all Mn-defect configurations considered here are not equally probable in our samples, the calculation of defect-formation energy is also carried out using the pseudo-potential SIESTA method by taking into account optimization of atomic positions [9, 13]. The calculated defect-configuration energies and magnetic properties are presented in table 1. The results show that the values of defect-formation energy have 1.3, 2.7, 3.0, and 3.9 eV for S, $2S$, $2S+I$ type 1, and $2S+I$ type 2 configurations, respectively. In the case of the $4S+I$ configuration, the formation energy (8.4 eV) is more than twice as high as the $2S+I$ configuration. This indicates that the formation of large $4S+I$ defects is highly elusive in our samples.

Figure 5 shows the calculated Mn 3d density of states (DOS) for Mn metal, MnO, and various Mn-defect configurations. Both S and $S+S$ configurations of Mn dopants in Cu_2O have well-separated valence and conduction bands, and exhibit fairly similar spectral features to that of MnO. However, as given in table 1, the exchange interaction (J) between Mn(S) atoms is antiferromagnetic (AFM) with a superexchange of about 4 meV and the magnetic moment

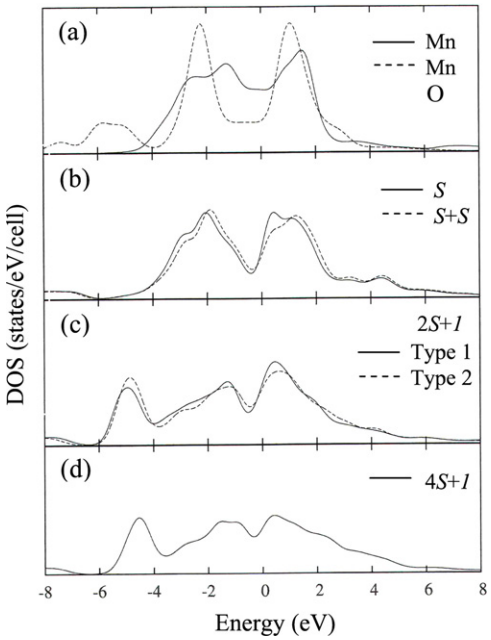

Figure 5. Calculated Mn 3d DOS for (a) Mn metal and MnO, and various Mn-defect configurations: (b) S and $S + S$ in Cu_2O, (c) $2S + I$ type 1 (solid line) and $2S + I$ type 2 (dashed line), and (d) $4S + I$.

on Mn atoms in the $S + S$ configuration (3.63 μ_B) is close to that in the S configuration (3.70 μ_B). For the $2S + I$ configurations (figure 5(c)), the Mn 3d DOS near the band gap is altered due to direct Mn–Mn bonds, but still shows the oxidation state. According to the XAS results shown in figure 1(a), the Mn oxidation state is estimated to be 2+. The calculation of magnetic properties of $2S + I$ type 1 defects gives a magnetic moment of 2.15 μ_B on Mn(S) and 1.02 μ_B on Mn(I) ions, resulting in an average magnetic moment of 1.09 μ_B. A smaller magnetic moment per Mn ion in Cu_2O than that in Mn oxide is typical of Mn-doped DMS materials because of antiferromagnetic Mn–Mn exchange interaction. We note that the $2S + I$ type 1 defect has a ferromagnetic (FM) exchange between Mn(S)–Mn(S) ions while the interaction between Mn(S)–Mn(I) is antiferromagnetic. On the other hand, magnetic moments of the $2S + I$ type 2 defect are reduced to 2.08 μ_B for Mn(S) and increases to 1.29 μ_B on Mn(I), which leads to a decrease of the average magnetic moment to 0.96 μ_B. The exchange interactions of this defect are −60 meV between Mn(S)–Mn(S) and −145 meV between Mn(S)–Mn(I).

From the obtained exchange values, we calculated the T_C for each defect configuration using a standard formula for the Ising model:

$$T_C = \frac{Ns(s+1)J}{3k_B}, \quad (1)$$

where N is the number of exchange pairs, s is the Mn spins, J is the exchange interaction, and k_B is the Boltzmann constant. In order to take into account long-range magnetic interactions (i.e. an interaction between configured defects), we calculated the T_C values by building a supercell containing two equivalent combinations of each defect configuration and also examined the difference in total energies between ferromagnetically and antiferromagnetically oriented combinations. The obtained T_C values are 408 K for a $2S + I$ type 1 and 218 K for $2S + I$ type 2. In addition, a ferromagnetically oriented combination is found to be more stable (8 meV lower total energy) than an antiferromagnetically oriented one for both $2S + I$ type 1 and type 2 defects. The similar change in T_C between $2S + I$ type 1 and type 2 defects to those between Mn-doped Cu_2O samples sintered at different temperatures suggests that at a sintering temperature of 650 °C, the $2S + I$ type 1 defects are the most likely ones to be formed and elevating the sintering temperature to 800 °C populates the $2S + I$ type 2 defects. This is also supported by lower defect-formation energy of type 1 than of type 2 defects.

In addition, different $I(L_2)/I(L_3)$ intensity ratios of resonant XES spectra relevant to CK transitions can be explained by considering free d carriers in the samples. Although the presence of Mn(I) atoms in both the 650 and 800 °C samples along with Mn(S) atoms is expected to increase the number of carriers (i.e. enhance the CK transitions), sintering at 800 °C promotes the formation of the $2S + I$ type 2 defect. This results in the suppression of CK transitions and thus the enhancement of the $I(L_2)/I(L_3)$ intensity ratio because the part of 3d carriers in the $2S + I$ type 2 defect should be involved in the Mn(S)–Mn(S) superexchange interaction via oxygen atoms. The reduced carriers in the 800 °C sample are well in accordance with resistivity measurements at RT. The 650 °C sample shows a resistivity of 1.38 Ω m, which is much lower than that of the 800 °C sample (6.47 Ω m).

In conclusion, we have investigated the electronic structure of Mn-doped Cu_2O bulk samples using soft x-ray emission spectroscopy and calculations based on a linear muffin-tin orbital method with the atomic sphere approximation. It has been shown that as well as substitutional Mn atoms, interstitial Mn atoms are present in ferromagnetic Mn-doped Cu_2O samples. These defects are responsible for a strong exchange interaction. A reduction in T_C with sintering temperature can be explained by the appearance of antiferromagnetic superexchange between substitutional Mn atoms via oxygen, which requires a higher defect-formation energy. This is accompanied by a decrease of magnetic moments, an increase of the $I(L_2)/I(L_3)$ intensity ratio in the Mn $L_{2,3}$ XES spectra, and a decrease in the number of carriers.

Acknowledgments

We gratefully acknowledge the Russian Academy of Sciences Programme (Project 01.2.006 13395). This work is also partly supported by the Russian Science Foundation for Basic Research (Projects 08-02-00148 and 06-02-16733), the Research Council of the President of the Russian Federation (Grants NSH-1929.2008.2) and the Natural Sciences and Engineering Research Council of Canada (NSERC), the Canada Research Chair programme and the EPSRC of the United Kingdom. D W Boukhvalov acknowledges support from Stichting voor Fundamenteel Onderzoek der Materie (FOM), The Netherlands.

References

[1] Dietl T, Ohno H, Matsukura M, Cibert J and Ferrand D 2000 *Science* **287** 1019

[2] Wei M, Braddon N, Zhi D, Midgley P A, Chen S K, Blamire M G and MacManus-Driscoll J L 2005 *Appl. Phys. Lett.* **86** 072514

[3] Kale S N, Ogale S B, Shinde S R, Sahasrabuddhe M, Kulkarni V N, Greene R L and Venkatesan T 2003 *Appl. Phys. Lett.* **82** 2100

[4] Liu Y L, Harrington S, Yates K A, Wei M, Blamire M G, MacManus-Driscoll J L and Liu Y C 2005 *Appl. Phys. Lett.* **87** 222108

[5] Pan L Q, Zhu H, Fan C F, Wang W G, Zhang Y and Xiao J Q 2005 *J. Appl. Phys.* **97** 10D318

[6] Ivill M, Overberg M E, Abernathy C R, Norton D P, Hebard A F, Theodoropoulou N and Budai J D 2003 *Solid-State Electron.* **47** 2215

[7] Sieberer M, Redinger J and Mohn P 2007 *Phys. Rev.* B **75** 035203

[8] Carvie L A J and Craven A J 1994 *Phys. Chem. Minerals* **21** 191

[9] Chang G S, Kurmaev E Z, Boukhvalov D W, Finkelstein L D, Kim D H, Noh T-W, Moewes A and Callcott T A 2006 *J. Phys.: Condens. Matter* **18** 4243

[10] Chang G S, Kurmaev E Z, Boukhvalov D W, Finkelstein L D, Colis S, Pedersen T M, Moewes A and Dinia A 2007 *Phys. Rev.* B **75** 195215

[11] Grebennikov V I 2002 *J. Surf. Invest.: X-ray, Synchrotron Neutron Tech.* **11** 41

[12] Andersen O K 1975 *Phys. Rev.* B **12** 3060

[13] Soler J M, Artacho E, Gale J D, Garsia A, Junquera J, Orejon P and Sanchez-Portal D 2002 *J. Phys.: Condens. Matter* **14** 2745